High-precision cavity-enhanced spectroscopy for studying the H-2-Ar collisions and interactions

N. Stolarczyk, G. Kowzan, F. Thibault, H Cybulski, M. Slowinski, Y. Tan, J. Wang, A. W. Liu, S. -M. Hu, P. Wcislo

Accepted to J. Chem. Phys. 10.1063/5.0139229

High-precision cavity-enhanced spectroscopy for studying the H_2-Ar collisions and interactions

N. Stolarczyk,[1,2,a)] G. Kowzan,[1] F. Thibault,[3] H. Cybulski,[4] M. Słowiński,[1] Y. Tan,[2] J. Wang,[2] A.-W. Liu,[2] S.-M. Hu,[2] and P. Wcisło[1]

[1)] *Institute of Physics, Faculty of Physics, Astronomy and Informatics, Nicolaus Copernicus University in Toruń, Grudziądzka 5, 87-100 Toruń, Poland*

[2)] *Hefei National Laboratory for Physical Sciences at Microscale, iChem center, University of Science and Technology of China, Hefei 230026 China*

[3)] *Univ Rennes, CNRS, IPR (Institut de Physique de Rennes)-UMR 6251, F-35000 Rennes, France*

[4)] *Faculty of Physics, Kazimierz Wielki University, al. Powstańców Wielkopolskich 2, 85-090 Bydgoszcz, Poland*

(Dated: 31 January 2023)

Information about molecular collisions is encoded in the shapes of collision-perturbed molecular resonances. This connection between molecular interactions and line shapes is most clearly seen in simple systems such as the molecular hydrogen perturbed by a noble gas atom. We study the H_2-Ar system by means of highly accurate absorption spectroscopy and *ab initio* calculations. On the one hand, we use the cavity-ring-down-spectroscopy technique to record the shapes of the S(1) 3-0 line of molecular hydrogen perturbed by argon. On the other hand, we simulate the shapes of this line using *ab initio* quantum-scattering calculations performed on our accurate H_2-Ar potential energy surface (PES). In order to validate the PES and the methodology of quantum-scattering calculations separately from the model of velocity-changing collisions, we measured the spectra in experimental conditions in which the influence of the latter is relatively minor. In these conditions, our theoretical collision-perturbed line shapes reproduce the raw experimental spectra at the percent level. However, the collisional shift, δ_0, differs from the experimental value by 20%. Compared to other line-shape parameters, collisional shift displays much higher sensitivity to various technical aspects of the computational methodology. We identify the contributors to this large error and find the inaccuracies of the PES to be the dominant factor. With regard to the quantum scattering methodology, we demonstrate that treating the centrifugal distortion in a simple, approximate manner is sufficient to obtain the percent-level accuracy of collisional spectra.

PACS numbers: Valid PACS appear here
Keywords: Suggested keywords

I. INTRODUCTION

Molecular hydrogen is a benchmark system for studying non-classical effects due to its large molecular rotational constant. Collisions involving H_2 display many atypical features, since H_2 does not provide any inelastic scattering channels at temperatures up to several hundred K[1]. Due to this fact, collision-induced spectroscopic effects in the molecular hydrogen spectrum are dominated by velocity-changing collisions[2]. Thus, the rovibrational lines of H_2 are strongly affected by the Dicke narrowing[3,4]. Moreover, the speed dependence of collisional broadening and shift[5,6] as well as their interplay with the velocity-changing collisions[4] are unusual in the spectral lines of molecular hydrogen.

Due to its simplicity, the H_2 molecule is accessible for the calculations from first principles, which, makes it a perfect system to study the entire methodology of *ab initio* line-shape calculations, from intermolecular potential-energy surfaces (PES) to the quantum scattering calculations, velocity-changing collisions models and spectral line-shape profiles[1,7–12].

Experimental measurements of the H_2-H_2 interaction, as well as interactions with noble gas atoms, have been performed for decades[13–17]. Recently, Perreault *et al.* measured rotationally-inelastic scattering of HD with molecular deuterium[18] and with helium atoms[19] in supersonic beams at 1 K. Subsequent quantum scattering calculations[20] found very good agreement with the measurements. In this paper, we report an analysis of a more complex system, i.e., H_2 perturbed by argon. The interaction with a 20-times-heavier perturber hampers the modeling of the velocity-changing collisions. Indeed, this problem has already been addressed in Refs.[4,9] and required a separate treatment of speed and velocity-changing collisions. Here, we adjust the experimental conditions in order to diminish the importance of the velocity-changing collision model and focus on the still-unresolved problem of the difference between the theoretical and experimental line shift[4].

This work analyzes the S(1) 3-0 transition in molecular hydrogen perturbed by argon. We perform highly accurate cavity ring-down spectroscopy (CRDS) measure-

[a)] Electronic mail: NikodemStolarczyk319@gmail.com, piotr.wcislo@umk.pl

Accepted to J. Chem. Phys. 10.1063/5.0139229

ments to collect the collision-induced spectral line shapes. Simultaneously, we perform fully *ab initio* quantum scattering calculations on our accurate H_2-Ar PES, to simulate the theoretical line profiles.

We consider several different approaches to describing the theoretical spectral line-shape profiles, gradually adding subsequent corrections to the model. Starting from the base case, we refine our methodology by: including the effects of centrifugal distortion in a simplified manner (simple CD), including a more complete treatment of centrifugal distortion (full CD), and including the effects of vibrational coupling (VC). Neglecting these effects in our calculations results in the 6% error of the pressure broadening and shift parameters, γ_0 and δ_0. (Note that error in other line-shape parameters has a much smaller impact on the resulting spectra[10]. Although for molecular hydrogen the effect of the Dicke parameter is non-negligible, its value is insensitive to CD and VC corrections.) Both the full CD treatment and inclusion of the VC significantly increase the complexity of the calculations. Additionally, for VC the computational cost is significantly increased relative to simpler cases. We find that just the inclusion of the simplified CD already accounts for the majority of the corrections and reduces the error in the line-shapes parameters from 6% to below 1%. This finding would result in a significant reduction of the numerical cost of future *ab initio* line-shape calculations. One should, however, perform additional tests prior to generalizing this observation to other transitions and molecular collisional systems.

While we achieve agreement at a level of 1.6% between theory and measurement in terms of the shape of the line, the experimental and theoretical values of the shift parameter, δ_0, differ by 20%. We consider various factors both on the theoretical and experimental side, to explain this discrepancy. We find that the δ_0 parameter is exceptionally sensitive to various computational aspects of our *ab initio* methodology and that the major contribution to this difference originates from inaccuracies of the PES.

II. CAVITY-ENHANCED MEASUREMENTS

We perform the cavity ring-down spectroscopy (CRDS) measurements of the S(1) 3-0 line of H_2 perturbed by Ar using the experimental setup presented in Fig. 1. We use a 1-m long optical cavity with a finesse equal to 63 000. The reflectivity of the cavity mirrors is 99.995% and one of the two mirrors is attached to a piezoelectric servomechanism in order to match the cavity modes with the probe laser frequency. We use a Ti:Sapphire laser source (Coherent 899-21) pumped by a 532-nm solid laser (Verdi-18). A beam from the probe laser after the acousto-optic modulator (AOM2) and the electro-optic modulator (EOM) is locked to a temperature-stabilized ($\Delta T \approx 10$ mK at 302 K) ultralow expansion (ULE) etalon with the Pound-Drever-Hall method[21]. In this way, the probe laser frequency could be tuned with sub-MHz resolution. The absolute frequency is calibrated by a wavemeter with an accuracy better than 10 MHz. The cavity ring-down spectra are recorded in step-scan mode. A single step usually consists of 100 ring-down events initiated by chopping the laser beam with the AOM1. We apply a least squares fitting procedure to fit the exponential curve to the ring-down signal to retrieve the absorption coefficient at a given point. See Refs. 22 and 23 for the detailed description of each subsystem of the setup.

The spectra are collected at room temperature for different proportions of the H_2 to Ar partial pressures, i.e., 1:1, 1:2, 1:4, and 1:7, with the H_2 pressure being kept 12.4 kPa. The accuracy of the pressure gauge is 1%.

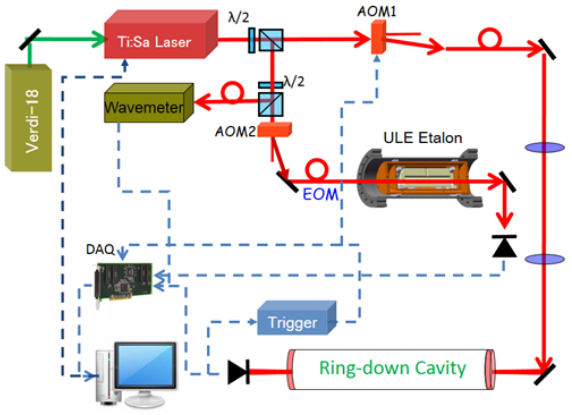

FIG. 1. Cavity ring-down spectrometer in Hefei laboratory. AOM and EOM are the acousto- and electro-optic modulators, respectively, and Verdi-18 is the laser source used for Ti:Sapphire laser pumping. The frequency of the laser is stabilized to the ultra-low-expansion (ULE) etalon, allowing us to reach the stability of 10 MHz.

III. *AB INITIO* LINE-SHAPE CALCULATIONS

This section discusses the theoretical analysis of the shape of the isolated S(1) 3-0 rovibrational spectral line of H_2 perturbed by Ar. We perform fully *ab initio* calculations within the framework of the generalized Hess method (GHM)[24–26]. In the following subsections, we provide details of the potential energy surface (PES), quantum scattering calculations, generalized spectroscopic cross sections, as well as calculations of the line-shape parameters and line-shape model.

A. Potential energy surface

We use our H_2-Ar potential energy surface (PES)[4] calculated by means of the spin-restricted coupled-cluster with single, double, and perturbative triple excitations [CCSD(T)] method employing the large aug-cc-pCVQZ

basis set[27–30]. This basis was further extended with a set of $3s3p2d2f1g1h$ midbond functions[31,32], denoted as 332211, with exponents of 0.90, 0.30, and 0.10 for s and p, 0.60 and 0.20 for d and f, and 0.30 for g and h functions that were placed in the middle of the van der Waals bond.

The interaction energies corrected for the basis set superposition error using the counterpoise (CP) method[33] were evaluated using the MOLPRO program 2010.1[34] and 2012.1[35] versions. In the calculations, all electrons were correlated.

To accurately reproduce features of the H_2-Ar PES, the calculations of intermolecular interaction energy were performed for 2 960 geometries of the system. The intermolecular distance R was varied in a range from 1.70 to 20.00 Å (37 points in total) covering some part of the repulsive wall (up to about 20 000 cm^{-1}), the entire van der Waals well and long-range (interaction energy slightly above -5×10^{-3} cm^{-1}) regions. The values of the θ angle were chosen to correspond to the abscissas of 9-point Lobatto-Gauss quadrature. In fact, because of the symmetry of the system, the calculations were done only for 5 different angles. The H-H bond length r_{HH} was stretched from 0.30 to 1.8 Å in steps of 0.10 Å.

Our PES is expanded in the basis of even Legendre polynomials up to the 8th order. To include the effects of centrifugal distortion (CD) and vibrational coupling (VC), the matrix elements for the collisional coupling between the rovibrational wavefunctions of H_2, $\langle \nu' j' | V_l(R, r_{HH}) | \nu'' j'' \rangle$, were calculated for $\nu', \nu'' = 0, \ldots, 5$ and $j', j'' = 1, 3, \ldots, 15$, where ν and j stand for the vibrational and rotational quantum numbers, while $'$ and $''$ mark the final and initial states, respectively.

Finally, we have repeated the PES calculations, taking into account relativistic effects. To do so, the CCSD(T) calculations were performed using the second-order Douglas-Kroll-Hess (DKH) Hamiltonian[36–38] with the aug-cc-pCVQZ-DK basis set[39]. The basis set was also enhanced with the 332211 midbond functions placed in the middle of the van der Waals bond. The calculations were done for all the 2 960 geometries of the system. In Sec. IV we compare the results obtained with these two versions of PES.

B. Generalized spectroscopic cross sections and spectral line-shape parameters

The scattering problem was solved at different levels of approximation to estimate the influence of CD and VC. In all the cases, S-matrices were obtained by solving the close coupling equations numerically[40,41] with the log-derivative propagator[42,43] using the MOLSCAT code[44]. The equations were propagated starting at either the separation distance, R set to 1.01 Å or 1.7 Å, but we found the differences between these two cases to be negligible. The maximum propagation distance was set to at least 20 Å. To determine whether it needs to be increased we calculated the position of the furthest classical turning point in the centrifugal potential, R_{cent}. If $2.5R_{cent}$ was larger than 20 Å, then the maximum propagation distance was set to $2.5R_{cent}$. We verified that increasing the distance beyond that point (e.g. to $4.0R_{cent}$) resulted in negligible differences. We obtained the values of $\langle \nu' j' | V_l(R, r_{HH}) | \nu'' j'' \rangle$ for $R > 20$ Å in two ways. For $\nu' = \nu''$, $l = 0$, the matrix elements were extrapolated with a simple phenomenological dependence, a/R^n, fitted in the 15 Å $< R <$ 20 Å region. In the remaining cases, the values of the matrix elements for distances approaching $R = 20$ Å were already negligible, therefore they were set to zero for R's beyond that point. The S-matrices were calculated at kinetic energies up to 2300 cm^{-1} at 286 points.

In the base case, in which the CD was not accounted for, the scattering equations were propagated for collisional matrix elements with $j' = j'' = 0$. Subsequently, CD was partially included by using the collisional matrix elements with $j' = j'' = 1$ in the ground vibrational state and with $j' = j'' = 3$ in the excited vibrational state. Finally, CD was fully accounted for by using the collisional matrix elements with j' and j'' matching the actual rovibrational levels included in the basis used to perform the calculations. In all the preceding cases, the scattering problem was solved separately in the ground vibrational manifold ($\nu' = \nu'' = 0$) for the initial radiative state $(\nu, j) = (0, 1)$ and in the excited vibrational manifold ($\nu' = \nu'' = 3$) for the final radiative state $(\nu, j) = (3, 3)$. The full CD calculations were subsequently expanded to include collisional coupling between different vibrational levels (VC). This was done by performing a separate set of calculations for the $(0, 1)$ state and the $(3, 3)$ state. The basis for scattering calculations in the former state included all open channels in the $\nu = 0, 1, 2$ vibrational manifolds and one closed channel in the $\nu = 0$ manifold. Similarly, the basis for the $(3, 3)$ state scattering calculations included all open channels in the $\nu = 1, 2, 3$ vibrational manifolds and one closed channel in the $\nu = 3$ manifold. The $\nu = 0$ state was not included because the matrix elements for the collisional coupling to that state from the $\nu = 3$ state were negligible.

Figure 2 shows the generalized spectroscopic cross sections, which are calculated directly from the S-matrices[25,45]. The depicted cross sections were calculated with relativistic corrections of the PES including relativistic corrections, full CD, and VC (the cross sections are appended in the Supplementary Material). Unless stated otherwise, all the calculations within this work were performed with these cross sections.

We use these cross sections (σ_0^q denotes the broadening and shift cross section, and σ_1^q denotes the Dicke cross section) to calculate the line-shape parameters: the speed-dependent pressure broadening, $\gamma(v)$, and shift, $\delta(v)$, as well as the complex Dicke parameter, $\widetilde{\nu}_{opt}$:

$$\gamma(v) + i\delta(v) = \frac{1}{k_{\rm B}T}\frac{v_{\rm pm}^2}{\pi^{3/2}cv}e^{-\frac{v^2}{v_{\rm pm}^2}} \int_0^\infty \sigma_0^q(v_i, j_i, v_f, j_f; E_{\rm kin} = xk_{\rm B}T)x^2 e^{-x^2} \sinh\left(\frac{2vx}{v_{\rm pm}}\right) {\rm d}x\,, \quad (1)$$

$$\widetilde{\nu}_{\rm opt} = \frac{1}{2\pi c}\frac{1}{k_{\rm B}T}\langle v_{\rm r}\rangle M_2 \int_0^\infty {\rm d}x\, xe^{-x}\left(\frac{2}{3}x\sigma_1^q(v_i, j_i, v_f, j_f; E_{\rm kin} = xk_{\rm B}T) - \sigma_0^q(v_i, j_i, v_f, j_f; E_{\rm kin} = xk_{\rm B}T)\right), \quad (2)$$

where c is the speed of light in vacuum, v is the active molecule speed, $v_{\rm pm}$ is the most probable perturber speed, $\langle v_{\rm r}\rangle$ is the mean relative speed of the colliding partners, $k_{\rm B}$ is the Boltzmann constant, T is the temperature and $M_2 = \frac{m_{\rm p}}{m+m_{\rm p}}$, with m and $m_{\rm p}$ being the masses of the active and perturbing molecules, respectively.

Figure 3 presents the speed dependences of the pressure broadening and shift obtained from the quantum-scattering calculations. The solid black curves present the *ab initio* speed-dependent pressure broadening and shift for the S(1) 3-0 transition in H_2 perturbed by Ar. The dashed lines mark the pressure broadening and shift parameters averaged over the Maxwell-Boltzmann speed distribution, i.e.,

$$\gamma_0 + i\delta_0 = \frac{1}{2\pi c}\frac{1}{k_{\rm B}T}\langle v_{\rm r}\rangle \int {\rm d}x\; xe^{-x}\sigma_0^q(v_i, j_i, v_f, j_f; E_{\rm kin} = xk_{\rm B}T). \quad (3)$$

To describe the H_2-H_2 collisions we make use of the line-shape parameters derived experimentally in Ref.[13] (see Table 2(f) therein). The parameters were reported within the quadratic approximation, i.e.,

$$\gamma(v) + i\delta(v) \approx \gamma_0 + i\delta_0 + (\gamma_2 + i\delta_2)\left(\frac{v^2}{v_{\rm m}^2} - \frac{3}{2}\right), \quad (4)$$

where[5,11]

$$\gamma_2 + i\delta_2 = \frac{v_{\rm m}}{2}\frac{\rm d}{{\rm d}x}\Big(\gamma(v) + i\delta(v)\Big)\Big|_{v=v_{\rm m}}, \quad (5)$$

with $v_{\rm m}$ being the most probable absorber speed. The red curves in Fig. 3 present the speed-dependent pressure broadening and shift for the self-perturbed H_2 S(1) 3-0 line, with the corresponding dashed lines marking γ_0 and δ_0 for this system.

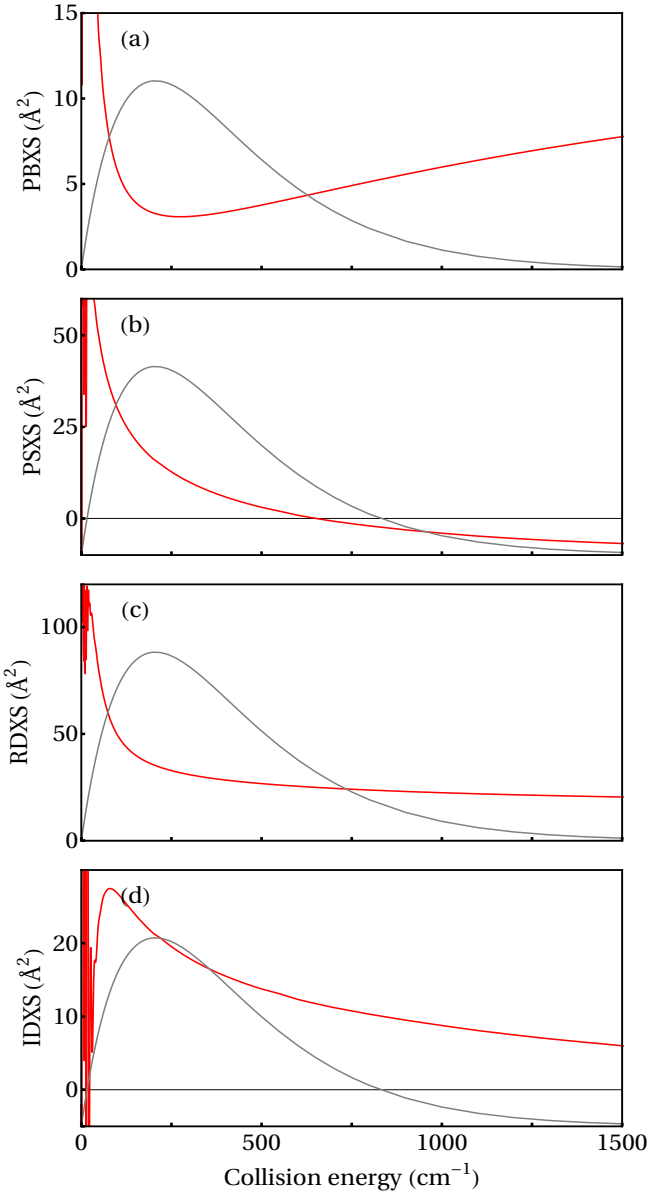

FIG. 2. Generalized spectroscopic cross sections for the S(1) 3-0 transition in H_2 perturbed by Ar are shown with red curves. (a) Pressure broadening cross-section, PBXS. (b) Pressure shift cross-section, PSXS. (c) Real part of the Dicke cross-section, RDXS. (d) Imaginary part of the Dicke cross-section, IDXS. The depicted cross sections are the results of the fully *ab intio* quantum scattering calculations with the relativistic PES, and the full CD and VC effects taken into account (the row (e) in Table I). To quantify the statistical contributions of different collision energies, we present the Maxwell-Boltzmann distribution of the relative absorber-perturber speed at $T = 296.65$ K (gray thin curves). We include the cross sections in numerical form in the Supplementary Material.

Accepted to J. Chem. Phys. 10.1063/5.0139229

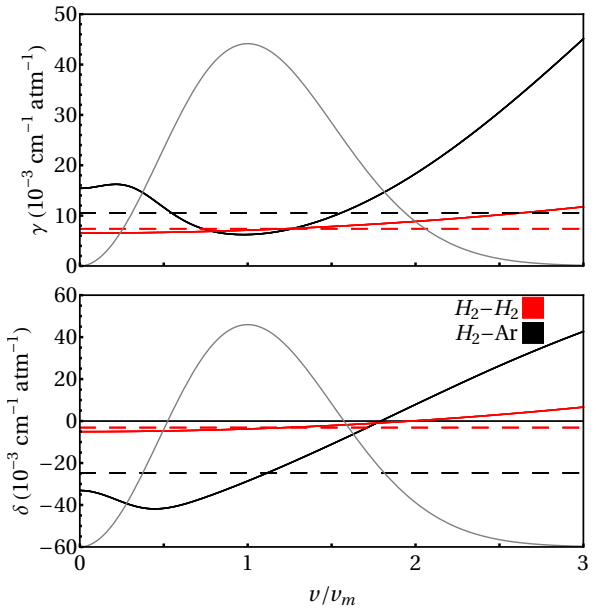

FIG. 3. Speed dependences of γ and δ for the S(1) 3-0 line in H_2 perturbed by Ar (black solid curves). We evaluate the exact speed dependence based on our fully *ab initio* quantum scattering calculations (the row (e) in Table I). For comparison, we plot the speed dependence of γ and δ for the self-perturbed H_2 (continuous red curves), based on Table 2 (f) of Ref.[13]. Dashed lines mark the speed-averaged values (i.e., γ_0 and δ_0, respectively) with the same color notation. With gray curves, we mark the Maxwell-Boltzmann distribution of molecule speed. The data is presented for $T = 296.65$K.

It is seen from Figure 3 that the H_2-Ar system displays a much stronger speed-dependence than H_2-H_2. Even though the speed-averaged broadening parameters are similar, their speed dependences vary significantly. The speed-dependent shift parameter is roughly ten times greater in the H_2-Ar system than in H_2-H_2.

Despite using the fully *ab initio* speed dependence of γ and δ for the H_2-Ar system, we also calculate the parameters of the quadratic approximation (γ_2 and δ_2) to quantitatively express the magnitudes of the speed dependences. The quadratic parameters are determined by the slope of the speed-dependent parameters at the most probable speed, Eq. (5). While the speed dependence of the shift is described well enough by the slope at this single point, this is not the case for the broadening. The speed-dependent broadening has a minimum near $v = v_\mathrm{m}$, see Fig. 3, hence the γ_2 parameter is close to zero, which does not reflect the actual strong speed dependence of $\gamma(v)$.

In Table I, we report the values of the six collisional line-shape parameters, i.e., the pressure broadening and shift, γ_0 and δ_0, their speed dependences, γ_2 and δ_2, and the real and imaginary parts of the Dicke parameter, $\widetilde{\nu}^r_\mathrm{opt}$ and $\widetilde{\nu}^i_\mathrm{opt}$. Rows (a)-(e) present the H_2-Ar parameters obtained with our fully *ab initio* calculations described in this section. Each subsequent row includes additional effects taken into account, i.e., the simplified and full CD, (b) and (c), relativistic PES corrections (rel), (d) and VC, (e). Row (f) presents the same parameters as row (e), however, δ_0 was adjusted to the experimental data, see Sec. IV B. The last row presents the H_2-H_2 parameters taken from Ref.[13].

Relativistic corrections to the PES as well as the CD and VC effects have a small impact on the line-shape parameters, see Table I. CD influences the line-shape parameters at the 2–6% level, except for $\widetilde{\nu}^r_\mathrm{opt}$, which is hardly influenced at all. Interestingly, the simplified form of CD is a good approximation to the full CD; the larger influence on γ_2 (3% change) is due to the atypical behavior of $\gamma(v)$, see the discussion regarding Fig. 3. The relativistic correction to the PES has a small impact (below 2%) on the values of the line-shape parameters (again, γ_2 does not well reflect $\gamma(v)$ due to its atypical speed dependence, see Fig. 3, and the large relative change in γ_2 has a small influence on the line shape). Similarly, VC has a very small (sub-percent) impact on the line-shape parameters. An important conclusion from the discussion on the theoretical results from Table I, from the perspective of quantum scattering calculations, is that it suffices to include only the simple CD (which does not add any numerical cost) to reduce the systematic theoretical error in the line-shape parameters from 6% to below 1% (here, we focus on γ_0 and δ_0 as they have the largest influence on the line shape; in the case of H_2 $\widetilde{\nu}^r_\mathrm{opt}$ has also a large influence on the line shape, but $\widetilde{\nu}^r_\mathrm{opt}$ is almost completely insensitive to the CD and VC corrections). This conclusion is crucial from the perspective of the optimization of the computational methodology since the inclusion of the VC increases the calculation time by a factor of ∼50.

C. Line-shape model

Our *ab initio* calculations allow us to simulate a complete line profile from first principles, with no collisional parameters fitted to the experiment. We fix all the Ar-induced collisional line-shape parameters at the values obtained from our quantum-scattering calculations, see row (e) in Table I.

To simulate the theoretical profiles, we make use of the billiard ball profile[46,47]. Within this model, the description of velocity-changing collisions is based on a hard-sphere approximation of the interaction potential. The billiard ball profile is superior to the commonly used hard- and soft-collision profiles as it allows one to take into account the mass ratio, α, between the collisional partners[10], which is especially important for the considered H_2-Ar system with $\alpha \approx 20$. In the case of such a large mass ratio, the relaxation of the velocity vector is described by two different rates[9]. The decays of its magnitude and direction are independent and require using two different time constants[9]. The hard- and soft-collision models fail in this case as they are both described by a single-parameter decay. We use the fully

TABLE I. Spectral line-shape parameters for the S(1) 3-0 line in H_2 (all the line-shape values are expressed in the units of 10^{-3}cm^{-1}atm^{-1}). The fully *ab initio* speed dependence of γ and δ for the H_2-Ar system was employed. We also list the γ_2 and δ_2, defined by Eq. (5), to quantitatively express the magnitude of speed dependence. The Doppler width at $T = 296.5$ K is $\omega_D = 64.0 \times 10^{-3}$cm^{-1}. Each row presents the parameters calculated with different effects taken into account: simple CD, full CD, relativistic effects in PES (rel), and VC. Letters (a)-(f) correspond to the annotations in Fig. 4

		γ_0	δ_0	γ_2	δ_2	$\widetilde{\nu}^{\mathrm{r}}_{\mathrm{opt}}$	$\widetilde{\nu}^{\mathrm{i}}_{\mathrm{opt}}$
(a)	without CD, rel, VC	10.5	-24.7	0.415	17.6	72.8	-15.6
(b)	simple CD	11.2	-25.8	0.405	18.2	72.3	-16.2
(c)	full CD	11.2	-25.9	0.390	18.2	72.3	-16.1
(d)	full CD + rel	11.2	-26.5	0.259	18.1	72.3	-15.8
(e)	**full CD + rel + VC**	**11.3**	**-26.4**	**0.347**	**17.8**	**72.1**	**-16.1**
(f)	H_2-Ar adjusted δ_0	11.3	-33.0	0.347	17.8	72.1	-16.1
	H_2-H_2, experimental[13]	7.2	-3.4	0.7	1.7	41.3	0.0

ab initio speed dependences of γ and δ (see Eq. (1)) for the Ar-perturbation contribution, while for the self-perturbation contribution we use the quadratic approximations taken from Ref.[13] (see Eq. (4)). These two contributions are proportional to the partial pressures of the two gases.

Since our experimental setup is not equipped with the absolute frequency reference, we fit the central frequency (the same value for all four pressures). We also fit the baseline, slope, and area of each of the four lines (separate values for each pressure). Since the lowest pressure of the experiment is below the applicability range of the direct diagonalization approach to the billiard ball profile calculations[11], we implemented the iterative approach[48] for the lowest pressure.

IV. EXPERIMENTAL VALIDATION OF THE THEORETICAL RESULTS

Figure 4 shows a direct comparison of our experimental and theoretical results. The top panel in the figure contains the measured points (black dots) and the theoretical spectral lines (red curves) calculated with the parameters from the row (e) in Table I. Panels (a)-(g) in Fig. 4 present the absolute residuals between the calculated and measured profiles, as well as the relative root-mean-square error (rRMSE), calculated within ±full width at half maximum (FWHM) from the line center.

A. Experimental validation of the fully *ab initio* model

Panels (a)-(e) in Fig. 4 show the residuals of the fully *ab initio* profile described in Sec. III. The theoretical line-shape model entirely originates from the first principles and no line-shape parameter was adjusted in this comparison.

We present several different approaches to describe the theoretical spectral line shape profiles, gradually adding subsequent corrections to the model. At each level of theory improvement, we obtain slightly different values of the spectral line-shape parameters, see Table I. While the parameters are modified by up to several percent, the corresponding differences in the line shapes (reflected by the rRMSE values) are well below a percent. The reason is twofold. On the one hand, the differences in the line-shape parameters are partially compensated by fitting the area and line position. On the other hand, the way the changes in line-shape parameters propagate on the spectra is not straightforward, this topic is covered in Appendix A of Ref. 10.

Similarly to the discussion on the line-shape parameters, see Sec. III B and Table I, the most significant improvement to the resulting line shapes is caused by taking into account the simple CD. Relativistic corrections to the PES, as well as including the full CD (in addition to the simple CD) and VC effects have almost no effect on the rRMSE. Again, the important conclusion is that reaching the sub-percent accuracy does not require taking into account the very computationally-expensive full CD and VC. Our most advanced fully *ab initio* model is in 2.65% agreement with experimental data, see panel (e) in Fig. 4.

B. *Ab initio* model with adjusted shift

The asymmetric shapes of the residuals in Fig 4 (a)-(e) indicate that the mismatch between the experimental and theoretical spectra is mainly caused by the incorrect value of the calculated pressure shift parameter, δ_0. Indeed, adjusting δ_0 in a multispectrum fitting procedure decreases the mean rRMSE to 1.58% and results in much smaller residuals, see panel (f) in Fig. 4. The experimental δ_0 parameter is 20% larger than the calculated value, see Table I. We analyze this discrepancy in Sec. V. The conclusion is that our fully *ab initio* calculations result in a 20% discrepancy in the δ_0 parameter compared to experimental spectra, but the collision-perturbed shapes of the experimental line are reconstructed at the 1%-level.

C. The role of the velocity-changing collision model

In this section, we benefit from having accurate experimental spectra and *ab inito* line-shape parameters to test the role of a velocity-changing collision model. In our ultimate *ab initio* simulation, Fig. 4 (e), we use an advanced, realistic line-shape model, i.e., the billiard ball profile[46,47]. In this section, we substitute the billiard-ball model with a simpler and widely-used hard-collision[49] profile that is much less computationally expensive, see Fig. 4 (g) (in panel (g) we use exactly the same values of the line-shape parameters and the full speed dependences as in (e) and only change the velocity-changing collisions model). It is clearly seen that this modification deteriorates the agreement with the experimental spectra, as quantified by the rRMSE increase from 2.65% to 3.7%.

It should be noted that in this work the theory-experiment comparison is done in the pressure range, in which the sensitivity to the velocity-changing collisions model is relatively small. At higher pressures, above the Dicke minimum, the velocity-changing collision model has a much larger influence. We discuss this issue in Appendix A, see also Fig. 5 and Ref. 4.

V. ANALYSIS OF THE DISCREPANCY IN PRESSURE SHIFT PARAMETER

We showed in Sec. IV B that, although our theoretical *ab initio* line-shape model accurately reproduces the shape of the experimental spectra, the calculated collision-induced line shift, δ_0, deviates from the experimental one by 20%. This section aims at providing an

Accepted to J. Chem. Phys. 10.1063/5.0139229

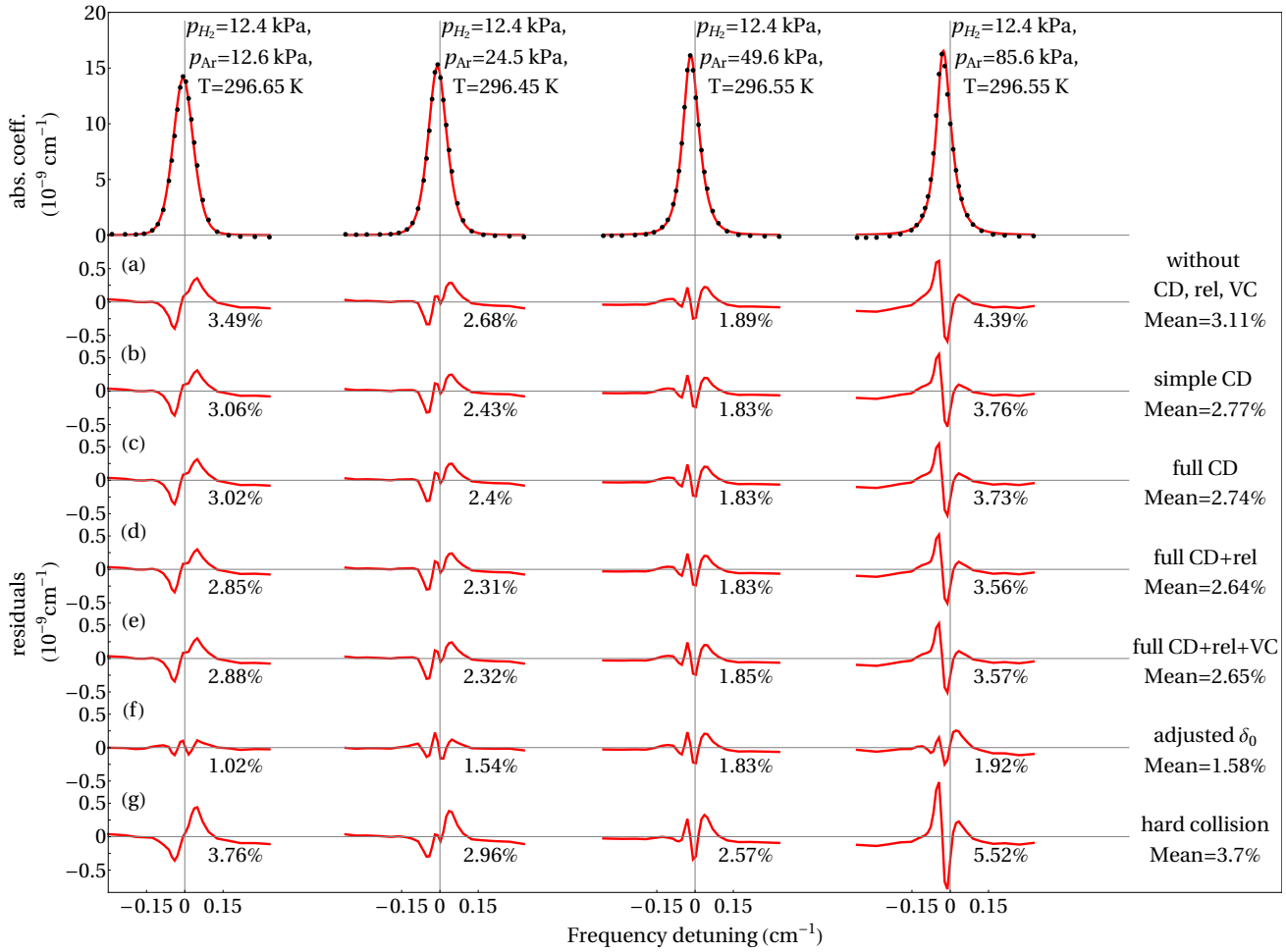

FIG. 4. The spectral line shapes of the S(1) 3-0 transition in H_2 perturbed by Ar. The top panel shows a direct comparison between the experimental (black dots) and fully *ab initio* (red curves) spectra. Panels (a)-(g) show the absolute residuals accompanied by the relative root-mean-square errors (rRMSE) calculated within ± FWHM of the line. The rightmost column contains the mean rRMSE of all pressures for a given model. Panels (a)-(f) correspond to the (a)-(f) rows of Table I and the spectra were calculated with the respective parameters. Panel (a) shows the residuals from the fully *ab initio* model without CD, VC, and relativistic PES corrections (rel). Subsequently, we include simple (b) and full (c) CD, vibrational coupling **VC** (d), and relativistic corrections to PES (e). In panel (f), we adjust the pressure shift parameter, δ_0, with a multi-spectrum fitting procedure. Panel (g) shows exactly the same comparison as panel (e), but the billiard-ball velocity-changing collision model is replaced with the hard-collision model.

explanation for this discrepancy. In Section V A, we estimate the uncertainty of the experimental δ_0, which is dominated by uncertainties of the *ab initio* line-shape model used in spectrum fits. In Section V B, we estimate the uncertainty of the calculated δ_0.

A. Uncertainty of the experimental δ_0

The measurement uncertainties that can affect the fitted δ_0, such as the inaccuracies of the frequency measurement or statistical uncertainties, are negligible in our case. The dominant contribution to the experimental uncertainty of δ_0 comes from the uncertainty of the fitted line-shape model. By distorting the line-shape model within the estimated confidence range, we estimate the corresponding uncertainty of δ_0.

To determine the experimental value of the δ_0 parameter, we simulate the fully *ab initio* billiard ball profile and fit δ_0, see row (f) in Table I and panel (f) Fig. 4. To determine the uncertainty of the fitted δ_0, we repeated the fit with the line-shape parameters distorted within their estimated confidence range. We include the influence of the three line-shape effects: the model of velocity-changing collisions, the narrowing and asymmetries related to the Dicke effect described by the complex Dicke parameter, $\widetilde{\nu}_{\rm opt}$, and the speed dependence of the pressure shift, δ_2 (the role of the speed dependence of the pressure broadening, γ_2, is negligible).

To estimate the uncertainties originating from the velocity-changing collision model, we substitute the kinetic-based billiard ball model with the phenomenological hard-collision model. Then we generate an *ab initio* profile with this simplified model and repeat the fit of δ_0. We obtain a 6% smaller value of the adjusted δ_0 in this way. The estimation of this uncertainty is conservative since the difference between the hard-collision and billiard-ball collision kernels is much smaller than the difference between the billiard-ball collision kernel and the actual one, see panels (c) and (d) in Fig. 2 in Ref. 9.

In the line-shape model, the operator of the velocity-changing collisions is scaled by the Dicke parameter. To estimate the uncertainty originating from the Dicke parameter uncertainty, we repeat the δ_0 fit with modified (within their uncertainty range) real and imaginary parts of the Dicke parameter. We obtained a 3% change in δ_0.

Similarly, to estimate the uncertainty originating from the uncertainty of the speed dependence of the pressure shift, δ_2, we repeat the fit with its value altered (within its uncertainty range), obtaining a 1% change in the fitted δ_0.

A minor role is played by the uncertainties of the measurement devices. The inaccuracy of the pressure gauge of 1% adds 1% uncertainty to the δ_0 parameter since δ_0 is obtained by dividing the actual shift by pressure. Additionally, the stability of the laser is 10 MHz $\approx 0.33356 \times 10^{-3}\text{cm}^{-1}$. The accuracy of the pressure shift parameter is directly connected to the frequency read, thus the maximum inaccuracy of δ_0 due to laser instability is 1%.

TABLE II. The budget of the experimental and theoretical uncertainties of the δ_0 parameter

Uncertainty contribution	u(δ_0)
Uncertainty of the experimental δ_0	
velocity-changing collisions model	6%
$\widetilde{\nu}_{\rm opt}$ uncertainty	3%
δ_2 uncertainty	1%
pressure measurement uncertainty	1%
laser maximum instability	1%
combined experimental uncertainty	**12%**
$\delta_0 = (-33.0 \pm 4.0) \times 10^{-3}\text{cm}^{-1}\text{atm}^{-1}$	
Uncertainty of the theoretical δ_0	
PES inaccuracy	21%
CC calculation convergence	1%
combined theoretical uncertainty	**22%**
$\delta_0 = (-26.4 \pm 5.6) \times 10^{-3}\text{cm}^{-1}\text{atm}^{-1}$	

Table II presents the full uncertainty budget. The top panel summarizes the uncertainty of the experimental δ_0. The uncertainty originating from the velocity-changing collisions model is dominant (6%) and the total combined uncertainty is 12%.

B. Uncertainty of the theoretical δ_0

Theoretical values of the line-shape parameters are obtained by performing quantum scattering calculations on our PES, as we described in Sec. III. The corresponding uncertainties of the quantum scattering calculations and the PES propagate to the uncertainty of the calculated δ_0.

To estimate the uncertainties originating from the close-coupling quantum scattering calculations, we repeat the calculations varying the numerical steps and other convergence parameters. The uncertainty of δ_0 estimated this way turns out to be smaller than 1%.

To estimate the uncertainty of δ_0 originating from the PES uncertainty, in the first step, we estimate the maximum inaccuracy of the PES. The inaccuracy of the PES can be estimated by the relative difference between the non-relativistic PES value and its best extrapolation to the complete basis set. The highest discrepancy turns out to be at the bottom of the PES well, where the difference between the PES (-54.39 cm^{-1}) and the extrapolated value is -0.72 cm^{-1}, which is 1.3%. We treat this value as the maximum inaccuracy of the PES. In the second step, we modify the PES by scaling the isotropic part of the potential in the upper rovibrational state by 1.3%. We find that such distortion of the PES results in

a 21% change of the theoretical δ_0 therefore we treat this value as our estimate of the uncertainty due to the PES inaccuracy, see Table II.

C. Combined uncertainties

The uncertainty budget of both theoretical and experimental values of the δ_0 parameter is summarized in Table II. Considering the uncertainties, we obtained the experimental $\delta_0 = (-33.0\pm4.0)\times10^{-3}\mathrm{cm}^{-1}\mathrm{atm}^{-1}$, and the theoretical $\delta_0 = (-26.4\pm5.6)\times10^{-3}\mathrm{cm}^{-1}\mathrm{atm}^{-1}$. The dominant contribution to the uncertainty budget results from the inaccuracies of the PES.

VI. SUMMARY

In this work, we focused on the S(1) 3-0 transition in molecular hydrogen perturbed by argon. We collected the experimental collision-induced spectral line shapes with the highly accurate cavity ring-down spectrometer of the Hefei laboratory. We also simulated the theoretical line profiles based on the fully *ab initio* quantum scattering calculations on our accurate H_2-Ar PES.

We verified the accuracy of several different approaches to model the theoretical line shapes, gradually adding subsequent corrections to our methodology. We considered the following effects: simplified centrifugal distortion (CD), full CD, and vibrational coupling (VC). We have found that neglecting these effects in our calculations resulted in a 6% error in the pressure broadening and shift parameters. Our numerical calculation revealed that the inclusion of the full CD and VC increased the calculation time by a factor of ∼50. We have shown that the simplified CD already accounts for the majority of the corrections and allows us to achieve a sub-percent error of the line-shape parameters.

While the theoretical and experimental spectra agreed within 1.58%, the measured and calculated shift parameters, δ_0, differed by 20%. We analyzed this discrepancy, from both the theoretical and experimental perspective, to find that the δ_0 parameter is exceptionally sensitive to some computational aspects of our *ab initio* methodology; we found that the major contribution to this discrepancy originated from the inaccuracies of the PES.

VII. SUPPLEMENTARY MATERIAL

The Supplementary Material to this work includes the generalized spectroscopic cross sections of the S(0) 3-0 transition of H_2 perturbed by argon, which was used in our analysis.

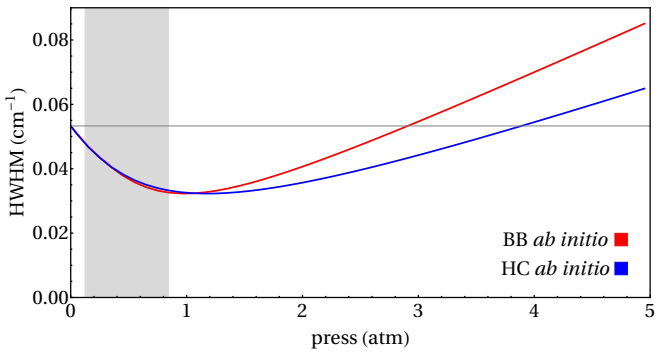

FIG. 5. Pressure dependence of the half width at half maximum (HWHM) of a spectral line. We consider two velocity-changing collision models: the *ab initio* billiard-ball model (BB *ab initio*) and the *ab initio* hard-collision model (HC *ab initio*). The gray zone marks the partial pressure range of Ar covered in our experiments. It is seen that in the range considered by us, the HWHM of the two line-shape models is almost the same.

VIII. ACKNOWLEDGMENTS

N.S. was supported by Polish National Science Centre Project No. 2019/35/N/ST2/04145. P.W. and M.S. were supported by Polish National Science Centre Project No. 2019/35/B/ST2/01118. G.K. was supported by National Science Center, Poland scholarship 2017/24/T/ST2/00242. Y.T. and S.M.H. acknowledge the support from the Chinese Academy of Sciences (XDC07010000). The research is a part of the program of the National Laboratory FAMO in Toruń, Poland. The project is co-financed by the Polish National Agency for Academic Exchange under the PHC Polonium French-Polish program (dec. PPN/X/PS/318/2018). Calculations have been partially carried out using resources provided by the Wroclaw Centre for Networking and Supercomputing (`http://wcss.pl`), Grant Nos. 294 and 546. We gratefully acknowledge Poland's high-performance computing infrastructure PLGrid (HPC Centers: ACK Cyfronet AGH, PCSS, CI TASK) for providing computer facilities and support within computational Grant No. PLG/2022/015576.

Appendix A: The role of the velocity-changing collisions

The line width of the H_2 molecule interacting with a heavier perturber strongly depends on the velocity-changing collision model,[4,8,50–53] see Fig. 5. To accurately reproduce the shape of a line, the velocity-changing model needs to include the absorber-to-perturber mass ratio.

A proper modeling of the velocity-changing collisions is of critical importance above the Dicke minimum (around 1.2 atm in the case of the S(1) 3-0 line considered in this

paper, see Fig. 5). In this regime, the direction of the velocity vector of an active molecule (here H_2) thermalizes much faster than its magnitude (speed).[4,9]. Hence, above the Dicke minimum, the Doppler broadening is eliminated and the main role is played by the speed-dependent effects, in particular, the inhomogeneous broadening due to the speed-dependence of collisional shift.[2]

Table 1 of Ref. 9 shows that the thermalization rate of speed strongly depends on the absorber-to-perturber mass ratio. In the case of velocity thermalization, this dependence is much weaker. Therefore, to model the velocity-changing collisions properly, one needs to take into account two different time constants, describing the speed and velocity decays independently, and including the dependence on the mass ratio.

The present paper, however, does not aim at studying the velocity-changing collisions (which was thoroughly covered in Refs. 9 and 4). Within this research, we focus on explaining the difference between experimental and theoretical δ_0. Hence, our goal is to reduce any additional uncertainties and inaccuracies coming from the velocity-changing collision model. Therefore we study the regime below the Dicke minimum, see the grayed area in Fig. 5, where the impact of the velocity-changing collision model is the least pronounced. The half-width at half maximum (HWHM) of the billiard-ball profile (that takes into account the mass ratio and the two different relaxation rates) and hard-collision profile is almost equal at the considered pressure range. The divergence of the two curves becomes clearly visible at higher pressures, above the Dicke minimum. Figure 4 reveals relatively small inaccuracy arising from a simplification of the velocity-changing model (compare the performance of the fully *ab initio* billiard-ball profile[46,47] (e) and the hard-collision profile[49] (g)).

[1] F. Thibault, P. Wcisło, and R. Ciuryło, "A test of H_2-He potential energy surfaces," Eur. Phys. J. D **70**, 236 (2014).

[2] N. Stolarczyk, P. Wcisło, and R. Ciuryło, "Inhomogeneous broadening, narrowing and shift of molecular lines under frequent velocity-changing collisions," J. Quant. Spectr. Radiat. Transfer **287**, 108246 (2022).

[3] V. G. Cooper, A. D. May, E. H. Hara, and H. F. P. Knapp, "Dicke narrowing and collisional broadening of the $S_0(0)$ and $S_0(1)$ Raman line of H_2," Can. J. Phys. **46**, 2019–2023 (1968).

[4] P. Wcisło, F. Thibault, H. Cybulski, and R. Ciuryło, "Strong competition between velocity-changing and phase- or state-changing collisions in H_2 spectra perturbed by Ar," Phys. Rev. A **91**, 052505 (2015).

[5] P. Wcisło, F. Thibault, N. Stolarczyk, H. Jóźwiak, M. Słowiński, M. Gancewski, K. Stankiewicz, M. Konefał, S. Kassi, A. Campargue, Y. Tan, J. Wang, K. Patkowski, R. Ciuryło, D. Lisak, R. Kochanov, L. Rothman, and I. Gordon, "The first comprehensive dataset of beyond-Voigt line-shape parameters from ab initio quantum scattering calculations for the HITRAN database: He-perturbed H_2 case study," J. Quant. Spectr. Radiat. Transfer **260**, 107477 (2021).

[6] N. Stolarczyk, F. Thibault, H. Cybulski, H. Jóźwiak, G. Kowzan, B. Vispoel, I. Gordon, L. Rothman, R. Gamache, and P. Wcisło, "Evaluation of different parameterizations of temperature dependences of the line-shape parameters based on ab initio calculations: Case study for the HITRAN database," J. Quant. Spectr. Radiat. Transfer **240**, 106676 (2020).

[7] F. Chaussard, X. Michaut, R. Saint-Loup, H. Berger, P. Joubert, B. Lance, J. Bonamy, and D. Robert, "Collisional effects on spectral line shape from the Doppler to the collisional regime: A rigorous test of a unified model," J. Chem. Phys. **112**, 158–166 (2000).

[8] H. Tran, F. Thibault, and J.-M. Hartmann, "Collision-induced velocity changes from molecular dynamic simulations in H_2–Ar: A test of the Keilson–Storer model and of line-broadening/shifting calculations for the Q(1) Raman line," J. Quant. Spectr. Radiat. Transfer **112**, 1035–1042 (2011).

[9] P. Wcisło, H. Tran, S. Kassi, A. Campargue, F. Thibault, and R. Ciuryło, "Velocity-changing collisions in pure H_2 and H_2–Ar mixture," J. Chem. Phys. **141**, 074301 (2014).

[10] M. Słowiński, H. Jóźwiak, M. Gancewski, K. Stankiewicz, N. Stolarczyk, Y. Tan, J. Wang, A.-W. Liu, S.-M. Hu, S. Kassi, A. Campargue, K. Patkowski, P. S. Żuchowski, R. Ciuryło, F. Thibault, and P. Wcisło, "Collisional line-shape effects in accurate He-perturbed H_2 spectra," J. Quant. Spectrosc. Radiat. Transfer **277**, 107951 (2022).

[11] P. Wcisło, F. Thibault, M. Zaborowski, S. Wójtewicz, A. Cygan, G. Kowzan, P. Masłowski, J. Komasa, M. Puchalski, K. Pachucki, R. Ciuryło, and D. Lisak, "Accurate deuterium spectroscopy for fundamental studies," J. Quant. Spectrosc. Radiat. Transfer **213**, 41 (2018).

[12] M. Słowiński, F. Thibault, Y. Tan, J. Wang, A.-W. Liu, S.-M. Hu, S. Kassi, A. Campargue, M. Konefał, H. Jóźwiak, K. Patkowski, P. Żuchowski, R. Ciuryło, D. Lisak, and P. Wcisło, "H_2-He collisions: Ab initio theory meets cavity-enhanced spectra," Phys. Rev. A **101**, 052705 (2020).

[13] P. Wcisło, I. E. Gordon, H. Tran, Y. Tan, S. M. Hu, A. Campargue, S. Kassi, D. Romanini, C. Hill, R. V. Kochanov, and L. S. Rothman, "The implementation of non-Voigt line profiles in the HITRAN database: H_2 case study," J. Quant. Spectrosc. Radiat. Transfer **177**, 75–91 (2016).

[14] W. K. Bischel and M. J. Dyer, "Temperature dependence of the Raman linewidth and line shift for the Q(1) and Q(0) transitions in normal and para-H_2," Phys. Rev. A **33**, 3113–3123 (1986).

[15] L. A. Rahn and G. J. Rosasco, "Measurement of the density shift of the H_2 Q(0–5) transitions from 295 to 1000 K," Phys. Rev. A **41**, 3698–3706 (1990).

[16] L. A. Rahn, R. L. Farrow, and G. J. Rosasco, "Measurement of the self-broadening of the H_2 Q(0–5) Raman transitions from 295 to 1000 K," Phys. Rev. A **43**, 6075–6088 (1991).

[17] W. E. Perreault, H. Zhou, N. Mukherjee, and R. N. Zare, "Resonant cold scattering of highly vibrationally excited D_2 with Ne," J. Chem. Phys. **157**, 144301 (2022).

[18] W. E. Perreault, N. Mukherjee, and R. N. Zare, "Quantum control of molecular collisions at 1 kelvin," Science **358**, 356–359 (2017).

[19] W. E. Perreault, N. Mukherjee, and R. N. Zare, "HD (v = 1, j = 2, m) orientation controls HD–He rotationally inelastic scattering near 1 K," J. Chem. Phys. **150**, 174301 (2019).

[20] M. Morita and N. Balakrishnan, "Stereodynamics of rotationally inelastic scattering in cold He + HD collisions," J. Chem. Phys. **153**, 091101 (2020).

[21] R. W. P. Drever, J. L. Hall, F. V. Kowalski, J. Hough, G. M. Ford, A. J. Munley, and H. Ward, "Laser phase and frequency stabilization using an optical resonator," Appl. Phys. B **31**, 97–105 (1983).

[22] C.-F. Cheng, Y. R. Sun, H. Pan, J. Wang, A.-W. Liu, A. Campargue, and S.-M. Hu, "Electric-quadrupole transition of H_2 determined to 10^{-9} precision," Phys. Rev. A **85**, 024501 (2012).

[23] C.-F. Cheng, Y. R. Sun, H. Pan, Y. Lu, X.-F. Li, J. Wang, A.-W. Liu, and S.-M. Hu, "Cavity ring-down spectroscopy of Doppler-broadened absorption line with sub-MHz absolute frequency accuracy," Opt. Express **20**, 9956–9961 (2012).

[24] S. Hess, "Kinetic theory of spectral line shapes. The transition between Doppler broadening and collisional broadening," Physica **61**, 80–94 (1972).

[25] L. Monchick and L. Hunter, "Diatomic-diatomic molecular col-

lision integrals for pressure broadening and Dicke narrowing: a generalization of Hess's theory," J. Chem. Phys. **85**, 713 (1986).
[26]G. C. Corey and F. R. McCourt, "Dicke narrowing and collisional broadening of spectral lines in dilute molecular gases," J. Chem. Phys. **81**, 2318–2329 (1984).
[27]T. H. Dunning, Jr., "Gaussian basis sets for use in correlated molecular calculations. I. The atoms boron through neon and hydrogen," J. Chem. Phys. **90**, 1007 (1989).
[28]R. A. Kendall, T. H. Dunning, Jr., and R. J. Harrison, "Electron affinities of the first-row atoms revisited. systematic basis sets and wave functions," J. Chem. Phys. **96**, 6796 (1992).
[29]D. E. Woon and T. H. Dunning, Jr., "Gaussian basis sets for use in correlated molecular calculations. III. The atoms aluminum through argon," J. Chem. Phys. **98**, 1358 (1993).
[30]K. A. Peterson and T. H. Dunning, Jr., "Accurate correlation consistent basis sets for molecular core-valence correlation effects: The second row atoms Al-Ar, and the first row atoms B-Ne revisited," J. Chem. Phys. **117**, 10548 (2002).
[31]F.-M. Tao and Y.-K. Pan, "Moller–Plesset perturbation investigation of the He_2 potential and the role of midbond basis functions," J. Chem. Phys. **97**, 4989 (1992).
[32]F.-M. Tao and Y.-K. Pan, "Ab initio potential energy curves and binding energies of Ar_2 and Mg_2," Mol. Phys. **81**, 507 (1994).
[33]S. F. Boys and F. Bernardi, "The calculation of small molecular interactions by the differences of separate total energies. some procedures with reduced errors," Mol. Phys. **19**, 553 (1970).
[34]H.-J. Werner, P. J. Knowles, G. Knizia, F. R. Manby, M. Schütz, *et al.*, "Molpro, version 2010.1, a package of ab initio programs," (2010), see: *http://www.molpro.net*.
[35]H.-J. Werner, P. J. Knowles, G. Knizia, F. R. Manby, M. Schütz, *et al.*, "Molpro, version 2012.1, a package of *ab initio* programs," (2012).
[36]A. Wolf, M. Reiher, and B. A. Hess, "The generalized Douglas-Kroll transformation," J. Chem. Phys. **117**, 9215 (2002).
[37]M. Reiher and A. Wolf, "Exact decoupling of the Dirac Hamiltonian. I. General theory," J. Chem. Phys. **121**, 2037 (2004).
[38]M. Reiher and A. Wolf, "Exact decoupling of the Dirac Hamiltonian. II. The generalized Douglas-Kroll-Hess transformation up to arbitrary order," J. Chem. Phys. **121**, 10945 (2004).
[39]W. A. de Jong, R. J. Harrison, and D. A. Dixon, "Parallel Douglas-Kroll energy and gradients in NWChem: Estimating scalar relativistic effects using Douglas-Kroll contracted basis sets," J. Chem. Phys. **114**, 48 (2001).
[40]A. M. Arthurs and A. Dalgarno, "The Theory of Scattering by a Rigid Rotator," Proc. Math. Phys. Eng. Sci. **256**, 540–551 (1960).
[41]M. S. Child, *Molecular Collision Theory* (Academic Press, 1974).
[42]D. E. Manolopoulos, "An improved log derivative method for inelastic scattering," J. Chem. Phys. **85**, 6425–6429 (1986).
[43]M. H. Alexander and D. E. Manolopoulos, "A stable linear reference potential algorithm for solution of the quantum close-coupled equations in molecular scattering theory," J. Chem. Phys. **86**, 2044–2050 (1987).
[44]J. M. Hutson and C. R. Le Sueur, "molscat: A program for non-reactive quantum scattering calculations on atomic and molecular collisions," Comput. Phys. Commun. **241**, 9–18 (2019).
[45]J. Schaefer and L. Monchick, "Line broadening of HD immersed in He and H_2 gas," Astron. Astrophys. **859**, 265 (1992).
[46]D. A. Shapiro, R. Ciuryło, J. R. Drummond, and A. D. May, "Solving the line-shape problem with speed-dependent broadening and shifting and with Dicke narrowing. I. Formalism," Phys. Rev. A **65**, 012501 (2002).
[47]R. Ciuryło, D. A. Shapiro, J. R. Drummond, and A. D. May, "Solving the line-shape problem with speed-dependent broadening and shifting and with Dicke narrowing. II. Application," Phys. Rev. A **65**, 012502 (2002).
[48]P. Wcisło, A. Cygan, D. Lisak, and R. Ciuryło, "Iterative approach to line-shape calculations based on the transport-relaxation equation," Phys. Rev. A **88**, 12517– (2013).
[49]D. Bohm and E. P. Gross, "Theory of plasma oscillations. A. Origin of medium-like behavior," Phys. Rev. **75**, 1851–1864 (1949).
[50]S. Green, "Raman Q-branch line shapes as a test of the H_2–Ar intermolecular potential," J. Chem. Phys. **93**, 1496–1501 (1990).
[51]S. Green, D. W. Schwenke, and W. M. Huo, "Raman Q-branch line shapes as a test of a H_2–Ar intermolecular potential," J. Chem. Phys. **101**, 15–19 (1994).
[52]L. Waldron and W.-K. Liu, "Hydrogen-rare Gas Interactions and Raman Line Shapes," J. Chin. Chem. Soc. **48**, 439–448 (2001).
[53]L. Waldron, W.-K. Liu, and R. J. Le Roy, "Collisional broadening and shifting of Raman lines, and the potential energy surface for H_2–Ar," J. Mol. Struct. THEOCHEM **591**, 245–253 (2002).

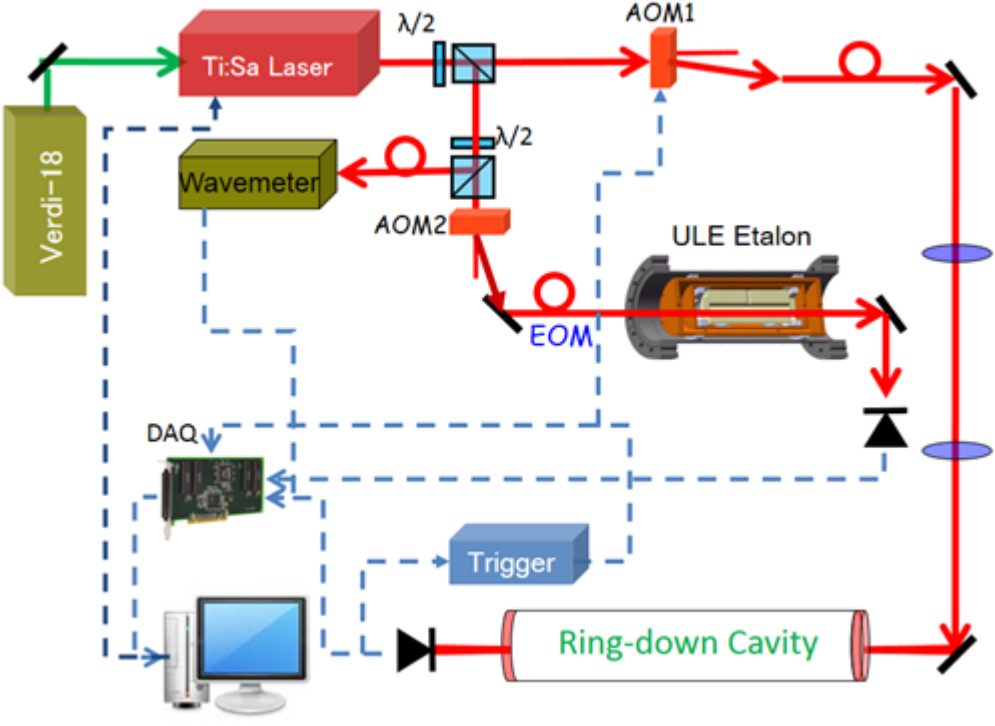
Ti:Sa Laser
λ/2
AOM1
Verdi−18
λ/2
Wavemeter
AOM2
ULE Etalon
EOM
DAQ
Trigger
Ring-down Cavity

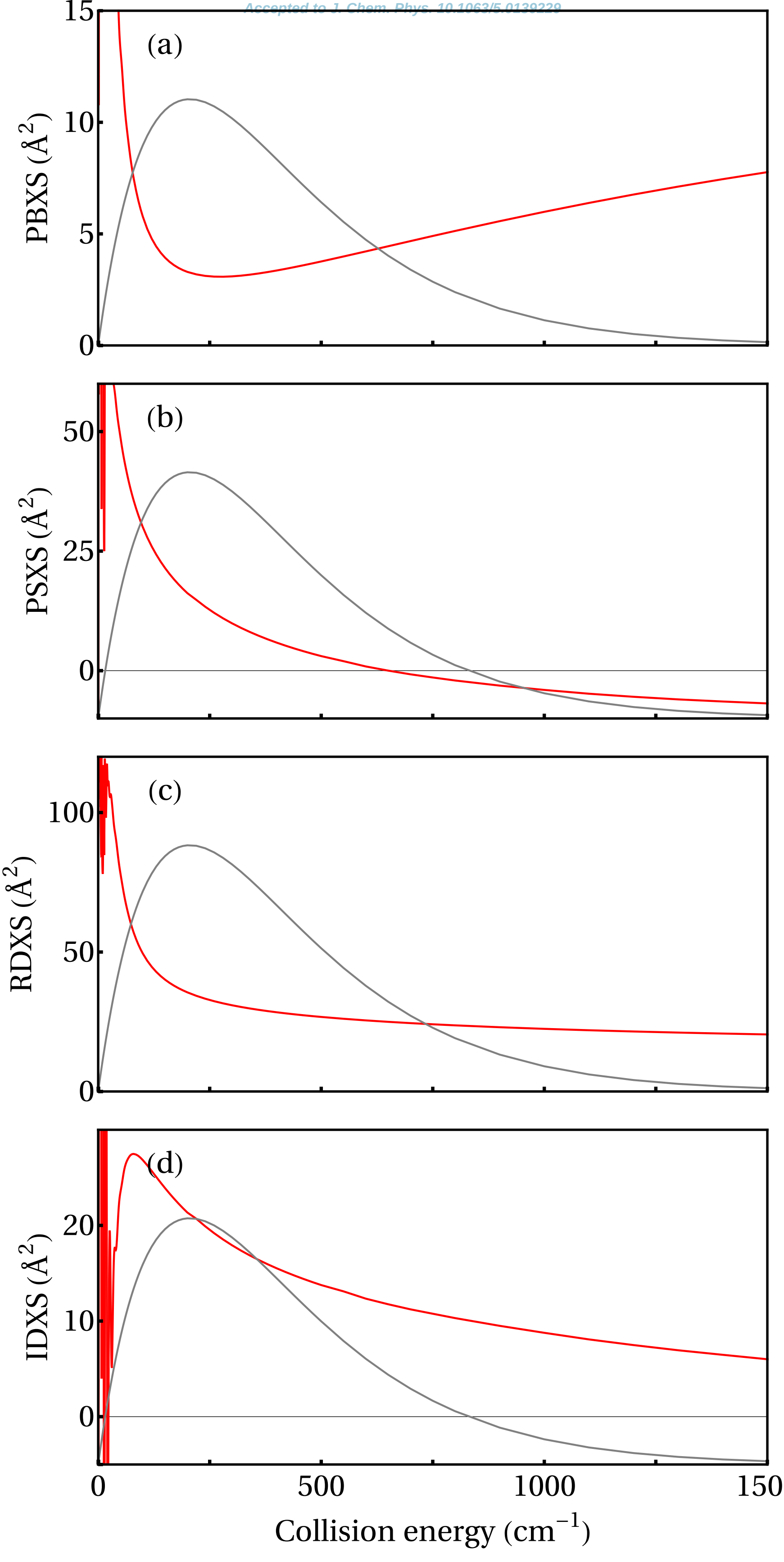

Accepted to J. Chem. Phys. 10.1063/5.0139229

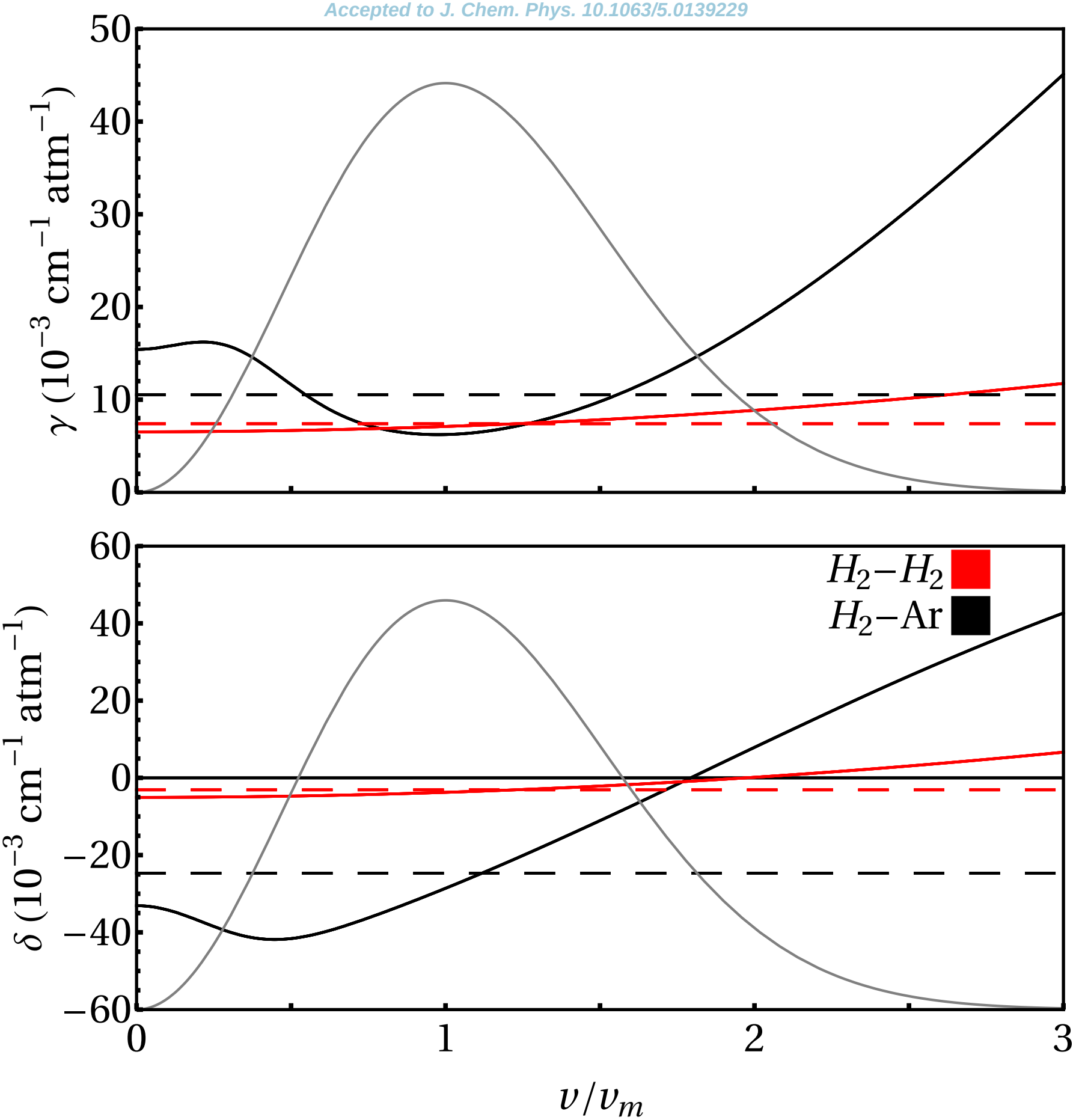

Accepted to J. Chem. Phys. 10.1063/5.0139229

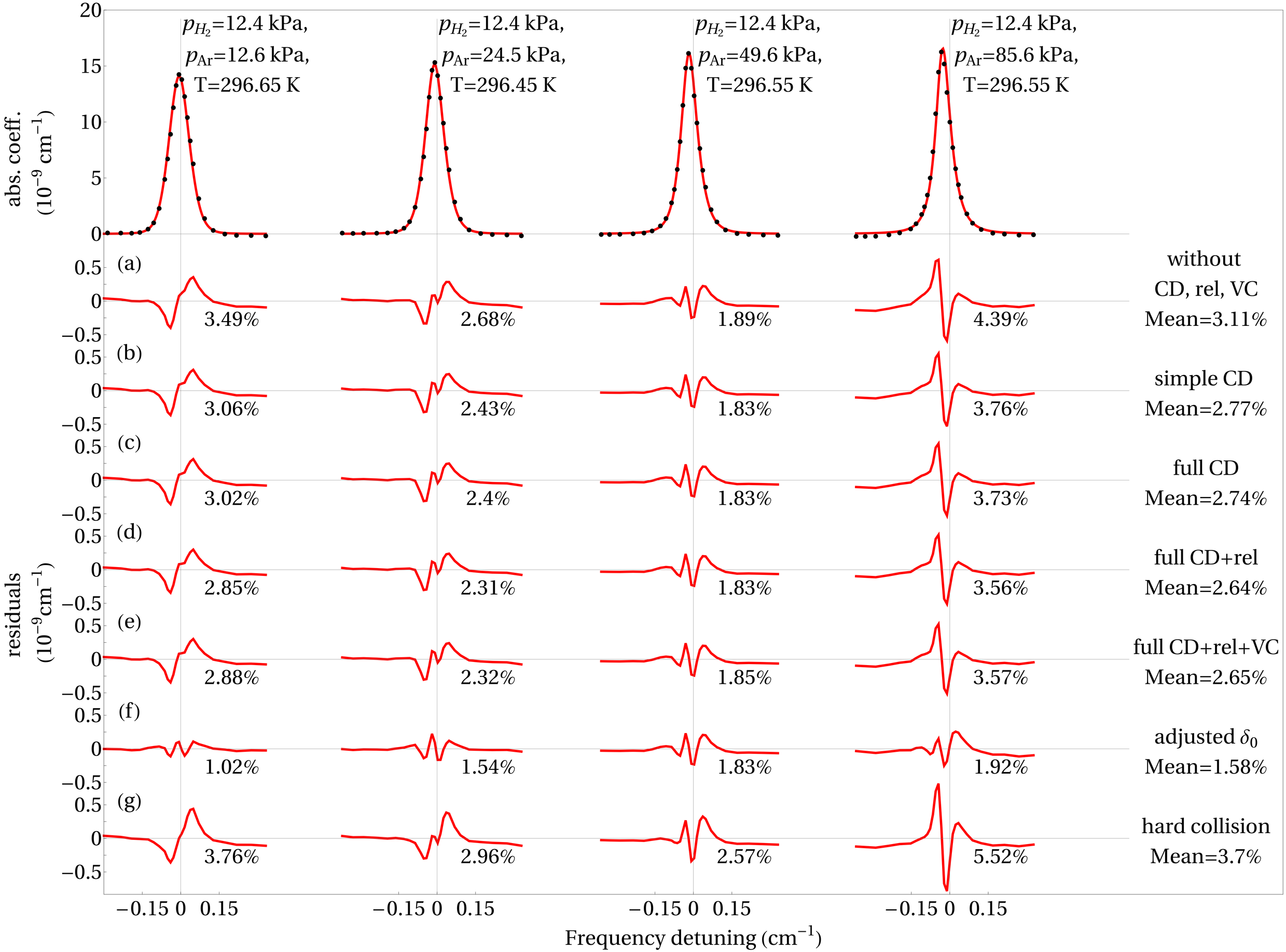

Accepted to J. Chem. Phys. 10.1063/5.0139229